

SecOComp: A Fast and Secure Simultaneous Compression and Encryption Scheme

Nivedita Shrivastava

Electrical Engineering Department
Indian Institute of Technology, Delhi, India
Email: nivedita.shrivastava@ee.iitd.ac.in

Smruti Ranjan Sarangi

Electrical Engineering Department
Indian Institute of Technology, Delhi, India
Email: srsarangi@cse.iitd.ac.in

Abstract—We live in a data-driven era that involves the generation, collection and processing of a massive amount of data. This data often contains valuable intellectual property and sensitive user information that must be safeguarded. There is a need to both encrypt and compress the data at line speed and sometimes with added power constraints. The majority of the currently available simultaneous compression and encryption (SCE) schemes are tailored for a specific type of data such as images for instance. This reduces their generic applicability. In this paper, we tackle this issue and propose a generic, efficient, and secure simultaneous compression and encryption scheme where the data is simultaneously encrypted using chaotic maps and compressed using a fast lossless compression algorithm. We claim that employing multiple chaotic maps and a lossless compression method can help us create not only an efficient encryption scheme but also compress the data efficiently in a hardware-friendly manner. We avoid all the known pitfalls of chaos theory based encryption that have prevented its widespread usage. Our algorithm passes all the NIST tests for nine different types of popular datasets. The proposed implementation uses 1.51x less storage as compared to the nearest computing work.

I. INTRODUCTION

The amount of digital data stored around the globe reached one zettabyte in the year 2012. This signified the beginning of a new era - the Zettabyte era. This data includes everything from healthcare databases to trained neural network (NN) models. Recent studies have projected an annual growth rate of 22% for the cloud data storage, which means that it will double in size every four years [1]. The International Data Corporation (IDC) forecasts that the world’s data will surpass 175 zettabytes by 2025, which will be more than triple the amount of data held in 2020 [2]. This data explosion is a result of the incorporation of intelligent agents that utilize machine learning and other forms of artificial intelligence to assess the rising amount of data generated by digital devices in our daily lives. This data is required during the development of driver assistance [7], autonomous car technologies [39], medical devices [44], IoT devices such as sensors in our bodies, homes, factories, and cities [33], high-resolution content for virtual and augmented reality [32], and 5G communication systems [22].

Even a trained neural network model with tens of layers and millions of nodes suffers from the problem of high data storage cost. The model size is increasing day by day. Recently proposed OpenAI’s ChatGPT [48] is one of the largest and

most powerful language processing models to date with 175 billion parameters. As the volume of data increases, it is imperative that we focus on the most cost-effective means of storing it, particularly in settings with resource constraints. This issue also bedevils cloud-based servers where throughput and latency considerations dominate.

To add to our woes, securing these data poses an additional concern as generating or acquiring this data is a costly affair. For an instance, acquiring raw data for training a neural network model itself can cost upwards of \$100K USD [53]. Thereafter, the know-how for the model and training process might be worth millions of dollars. This makes the trained model parameters as well as the consolidated raw data an attractive target for adversaries. Data is power, and if it is obtained by the wrong people, it can be used as a lethal weapon. Considering the amount of data generated today, it is crucial that we concentrate on techniques that can concurrently compress and encrypt the data since this will result in a significant reduction in compression and encryption overheads.

Sadly, the research area of simultaneously looking at compression and encryption of data has mostly focused on securing images. These approaches perform encryption using image-based characteristics, which limits their applicability to a broader domain. Another difficulty is that these algorithms are built for small-size data; hence, they are unsuitable for large data sets. Moreover, performing encryption and compression separately leads to additional overheads. For an instance, encryption-then-compression (ETC) is an unacceptable scheme as encryption decreases data redundancy and increases randomness, which negatively impacts the compression efficiency. Another option, compression-then-encryption (CTE), is a slow method due to the sequential nature of compression algorithms. Moreover, the difficulty of cracking the CTE scheme is equivalent to the difficulty of breaking the encryption algorithm.

All of these factors underscore the necessity for a simultaneous compression and encryption (SCE) solution that is efficient and is applicable to big data as well. In this work, we propose a variant of *chaos-based encryption-compression*, which offers robust performance and security guarantees while retaining a reasonable compression ratio. We utilize *zstd*, a fast lossless compression technique introduced by Facebook in 2016 for real-time compression scenarios.

Despite the prominence of chaos theory in the last decade, its impact on security research has been minimal. This is because of three factors: ① The chaos-based approaches rely on extensive real number arithmetic, making practical implementations onerous. ② The implementations were typically slow. ③ The schemes were cryptographically weak and were prone to several attacks [68], [46], [12]. Many researchers examined existing chaotic maps and demonstrated that if the chaotic performance is subpar, the maps become less secure [68], [62]. Wang et al. [62], [37], [38], and Xi et al. [68] pointed out flaws in the encryption schemes based on simple 1-D chaotic maps. All of these factors had a negative impact on the acceptance of chaos-based encryption techniques.

However, the past three years have witnessed a *resurgence* [55],[64],[41],[34],[47],[65],[66],[51][14],[17],[56],[21],[5], especially in the hardware community primarily because of the emergence of new improved algorithms. More intricate high-dimensional chaotic maps have been proposed [65], [5] in 2021, which can offer high levels of security guarantees. Using these newly proposed chaotic maps, several authors [4], [63] have created more secure chaos-based encryption techniques that rely on multiple chaotic maps. Although these algorithms proved to be resistant to a variety of attacks, they had substantial performance overheads. We found that these techniques are not intended for handling a lot of data. For example, when used to encrypt other large datasets, the encryption scheme proposed by Wang et al. [65] is very slow because of its highly sequential design ($24\times$ slower than our scheme *SecOComp*). To solve this problem, we rely on the work by Zhang et al. [69] and Lahcene et al. [45] who proposed an optimized fixed-point *Henon* and *Lorenz* map based design that is optimized for FPGAs, albeit in a generic context. This solved our performance issues because such algorithms are parallel, realizable on hardware, and also use fixed-point arithmetic.

We also took a thorough look at all the recent attacks that are proposed to break the chaos-based encryption algorithms [36], [38], [42]. Our selection of a specific combination of chaotic maps was based on an extensive examination and analysis of all the popular and relevant attacks. *We found that no attack has been developed for a chaos-based encryption system that incorporates 1D, 2D, and 3D chaotic maps. The majority of attacks are trivial and target very simple 1D chaotic maps like the Logistic map* [37], [36]. There is a body of theoretical work now that has generalized the space of attacks on chaos-based methods. Some generic properties have been identified – if an algorithm satisfies any of these properties then it is deemed to be vulnerable. One such work is proposed by Chen et al. [12]. They argue that the conventional approach where a chaotic map is used to generate pseudorandom numbers and the ciphertext is a XOR of this sequence and the plaintext, does not provide bulletproof security. To address all of these issues, we use three different non-trivial, multi-dimensional maps that have till date not been broken, we do not exclusively rely on the XOR operation, we permute the data based on the key. **We believe that this choice of design decisions steers clear of all**

known attacks (incl. foreseeable extrapolations) and does not satisfy any of the properties of algorithms that make it vulnerable (as identified in highly cited prior work).

Now, coming to the advantages of chaos-based encryption, we need to understand that it has distinct steps: first perform a permutation and then perform substitutions [5]. The permutation preserves the data statistics, which can be exploited for compression [5]. Naturally, this makes chaos-based algorithms better candidates for SCE.

As of today, the performance and security guarantees of software implementations of CTE and SCE [5] algorithms for images have been extensively analyzed. This paper proposes a novel chaos-based encryption-compression technique for big data. In addition, we also designed and implemented an efficient HW circuit that pre-computes and generates chaotic maps in the shadow of DRAM reads and compression engine operations, which leads to a much faster execution time.

The **main contributions in this paper** are as follows:

- ① Elaborate characterization of various chaotic maps and compression algorithms for NN workloads.
- ② Insights from the characterization section to find the right combination for designing a low-overhead and fast SCE algorithm to efficiently compress and encrypt the weights.
- ③ A novel permutation scheme using the *MergeShuffle* algorithm.
- ④ A novel highly-parallel HW design of the SCE engine, where we overlap the shuffling process with the compression operation to make the design faster. We also pre-compute the chaotic maps parallelly in the shadow of DRAM writes and the compression process.
- ⑤ A rigorous experimental and security analysis.

We have considered nine different types of datasets: neural networks, images, Kaggle datasets (Chatbots, medical data, etc). We shall extensively analyze pre-trained and quantized NN model data. The additional results of other datasets, which are quite similar, are also summarized at the end of Evaluation section. Our algorithm has been publicly accessible since Feb, 2023, and even after popularizing the algorithm, nobody has been able to propose a successful attack.

The text is divided into 8 sections. §II provides the background. §III outlines an attack on a CTE scheme. §IV provides a characterization of compression and encryption schemes. §V presents the proposed hardware design, §VI presents the performance results, §VII presents the security analysis and §VIII presents the related work. We finally conclude in §IX.

II. BACKGROUND

In this section, we present the relevant background.

A. Chaotic Maps

A chaotic map [50] is a discrete/continuous multi-dimensional map (multi-dimensional matrix) with a very high dependence on initial conditions. Some excellent properties of chaotic maps, such as sensitivity to initial conditions, pseudorandomness, ergodicity, and a large system parameter space, make them a popular choice for designing an encryption algorithm.

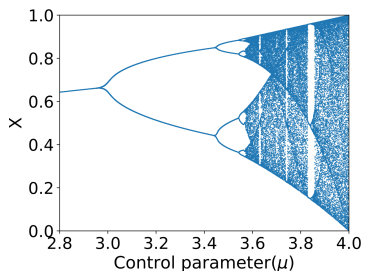


Fig. 1. The Bifurcation diagram for the *Logistic* map

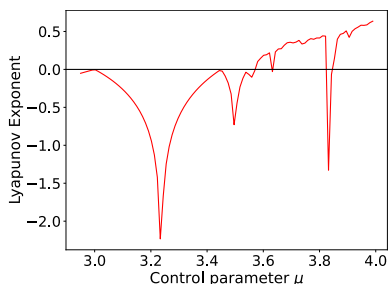


Fig. 2. Variation of the Lyapunov exponent with the control parameter for the *Logistic* map

The idea that chaotic systems are sensitive to initial conditions indicates that minuscule variations in initial conditions result in significant long-term variations. This is one of the defining features of chaos. We explain the basics of chaotic maps using a *Logistic* map. We represent the *Logistic* map using the equation $x_{i+1} = \mu x_i(1 - x_i)$, as shown in Table I. The new value, denoted by x_{i+1} , is determined by the previous value, x_i , as well as the control parameter μ . A slight fluctuation in μ results in long-term changes in the map. This behaviour is illustrated in Figure 1, which shows the bifurcation diagram for the *Logistic* map that demonstrates how the values of one of the variables of a chaotic map change as the control parameter is varied.

The diagram indicates that fixed values are attained only when $\mu \leq 3$. When $\mu = 3.1$, a bifurcation is visible on the map. The computed value oscillates. When $3.4 \leq \mu \leq 3.5$, the expected value oscillates between four distinct values as shown in Figure 1. As the value of μ increases, the set of values continue to multiply until chaotic behavior sets in (all possible values within the range subject to the real number resolution). We can clearly see that chaotic behavior sets in when $\mu \geq 3.6$.

The chaotic maps that we consider are shown in Table I.

1) *Lyapunov Exponent (LE)*: It serves as a measure of the sensitivity and predictability of the dynamic system with respect to changes in its initial conditions. A zero LE indicates that a system has reached the steady state. However, a negative LE indicates that a system has asymptotic stability. Any system with a positive LE is a chaotic system. For a discrete time chaotic map $x_{n+1} = f(x_n)$, LE (λ) is calculated as $\lim_{N \rightarrow \infty} \frac{1}{N} \sum \ln \left| \frac{dx_{n+1}}{dx_n} \right|$

Chaotic Map	Equations
Henon [67]	$x_{i+1} = 1 + y_i - ax_i^2; y_{i+1} = bx_i$
Tent [16]	$x_{i+1} = \mu x_i$ if $x_i < 1/2$; $x_{i+1} = \mu(1 - x_i)$ if $x_i > 1/2$
Logistic [50]	$x_{i+1} = \mu x_i(1 - x_i)$
Lorenz [45]	$x_{i+1} = \sigma(y_i - x_i); y_{i+1} = x_i(\rho - z_i) - y_i;$ $z_{i+1} = x_i y_i - \beta z_i$
Chirikov [13]	$x_{i+1} = x_i + k \sin(y_i); y_{i+1} = y_i + x_{i+1}$

TABLE I

CHAOTIC MAPS USED IN THE PAPER. (X, Y, Z) REPRESENTS MAP VALUES WHILE OTHER VARIABLES REPRESENT CONTROL PARAMETERS.

Figure 2 illustrates how the LE varies with the control parameter for the *Logistic* map. We can see that the LE approaches a positive value as soon as chaos sets in ($\mu \geq 3.6$).

While encrypting using chaotic maps, the **secret key** is a combination of the initial value of x and the value of control parameters (within a pre-defined range).

B. Compression Techniques

Modern compression algorithms rely on a combination of traditional compression methods such as the following.

Huffman encoding translates the data into unique binary codes. The binary code for the character with the highest frequency is the shortest, while the one with the lowest frequency is the longest.

LZ-77 Encoding uses the sliding window concept to reference previously read data/phrases. If a word/phrase is repeated, the previous occurrence is marked with a reference point (dictionary-based scheme).

Run-Length Encoding Repetitive symbols in the data are replaced with a *special character*, a *symbol*, and the *binary count* of the matching repetitive string. Each repeating string is represented by three fields: special character, symbol, and count. Table II presents a short description of the modern compression algorithms.

Algo.	Version	Based on
deflate [19]	1.10	LZ77, Huffman coding
bzip2 [57]	1.0.8	Burrows-Wheeler algo., Huffman Coding
lzma [35]	5.2.5	Sliding window technique of LZ77
zstd [15]	1.4.5	LZ77, Huffman or run-length encoding

TABLE II

VARIOUS LOSSLESS COMPRESSION LIBRARIES USED IN THE WORK

C. NIST Test

The NIST [59] test suite is the gold standard for testing the security of encryption algorithms. This test is widely used to test the efficiency of various encryption ciphers including AES [54]. The NIST test suite comes with 15 tests [59] as shown in Table III. The details of the tests have been explained in detail by Marton et al. [43]. Each test assesses whether the ciphertext appears to be random and whether it yields any statistical information about the corresponding plaintext, data patterns and the key. The test generates a p -value that indicates whether the ciphertext would be considered as random or not. It is regarded as random if the p -value exceeds a pre-specified significance level α (typically 0.01).

Test Name	Rep.	Test Name	Rep.
Frequency	T0	Overlapping	T8
BlockFrequency	T1	Universal	T9
CumulativeSums	T2	ApproximateEntropy	T10
Runs	T3	Random Excursion	T11
LongestRun	T4	Random Excursion Variant	T12
Rank	T5	Serial	T13
FFT	T6	LinearComplexity	T14
Nonoverlapping	T7		

TABLE III
NIST TEST SUITE

III. AN ATTACK ON CTE

Notation- Let the victim’s data P (of size S_P) be fed into the CTE engine. In a typical CTE algorithm, the compression engine compresses P to produce intermediate compressed data P_C , which is then sent to the AES engine to produce the final crypto-compressed data C of size S_C .

Threat model- The victim and attacker processes are executing on a system where the last level cache is shared. The attacker does not have access to P , P_C or the encryption key (K). She has access to S_P and S_C by analyzing the memory traffic. She can also access C . The attacker knows the type of encryption scheme, but not the compression scheme. The objective of the attack is to recover K and P . This is the standard threat model.

Attack- As the compressed data is encrypted, the attacker needs to first break the encryption. She can deduce the compression ratio by comparing the initial and final output sizes and the secret key using a timing-based side channel attack. Let us elaborate.

AES-128 does 10 rounds of encryption; rounds 1-9 encrypt the data using T-tables T_0, T_1, T_2, T_3 . The final round is special as it uses a distinct T-table T_4 ; this provides the added benefit of reduced noise. The final round ciphertext is computed as : $C_i = k_i \oplus T_4[j]$, where i represents the byte of the subkey and j represents the T-table index. An attacker will monitor T-table lookups (using prime-probe or similar attacks) and will guess the key byte k_i as z . If the guess is correct then the equation: $j = T_4^{-1}(C_i \oplus z)$ will be satisfied. In this way an adversary will be able to successfully retrieve the subkey similar to the previous works [10].

Our experiments show that the *inception* net model of size 25 MB can be compressed to 8 MB which requires 500K AES-128 encryptions, which is enough to successfully mount a side-channel attack. Even the smallest NN, *shufflenet*, requires 53k encryptions, which is sufficient for mounting an attack (as per prior work).

After obtaining the subkey, an attacker can reverse-engineer the original key (refer to [9]). Since she has both the key and the ciphertext, retrieving P_C is simple. The attacker now has access to the compression ratio and P_C . She can obtain P by determining the type of compression algorithm. This is a solved problem [8]; most solutions use NNs to deduce the algorithm out of a known set of algorithms.

In contrast to this, our scheme provides multi-level security by adding an additional permutation layer before the

compression stage and a substitution layer after compression. Additionally, we generate the chaotic maps simultaneously, which distorts the micro-architectural hardware signature of the map generation process. This reduces the chances of side-channel attacks because of the added noise [52].

IV. CHARACTERIZATION OF COMPRESSION ALGORITHMS AND CHAOTIC MAPS FOR CNN MODELS

We characterize the behaviour of different compression algorithms using the setup mentioned in Table IV. We executed different NN benchmarks, which are pre-trained and quantized for the ImageNet dataset. We used quantized models from the PyTorch Torchvision framework (see Table V). The benchmarks are chosen based on the availability of the pre-trained and quantized model; this is to ensure that our evaluation is realistic. We would like to add that *SecOComp* will work efficiently for models of any size.

Hardware Settings	
Intel Core i5-8300H CPU, 2.3 GHz	DRAM: 8 GB
#CPUs: 8 Cores	L1:128 KB, L2:1 MB, L3:8 MB
Software Settings	
Linux kernel: 5.15	Operating System: Ubuntu 20.04
Python version: 3.8	Pytorch version: 1.11
GCC: 9.4	Boost version: 1.71

TABLE IV
SYSTEM CONFIGURATION FOR SOFTWARE CHARACTERIZATION

A. Characterization of Compression Algorithms

We examine the compression ratio and the compression time for the following lossless compression algorithms: *zstd*, *deflate*, *zlib*, *bzip2*, and *lzma*. As the algorithms are lossless, the accuracy of the NN models will not be affected; hence, accuracy analysis is unnecessary. We estimate the **compression ratio** which is the ratio between the size of the original model and the compressed model, as well as the compression time, as shown in Figures 3 and 4.

We found that the *bzip2* algorithm gives the best compression ratio while *zstd* gives the best compression time. We observe that the compression time is proportional to the model size. Although *zstd* does not provide the best compression ratio, but the ratio is still comparable with the other algorithms. Additionally, *zstd* is $7.49\times$ faster than *bzip2*. Moreover, *zstd* is only $1.27\times$ worse than *bzip2* with respect to the compression ratio. Thus, we decided to use *zstd* for compressing NNs owing to its superior performance.

Benchmark	Model (MB)	Size	Benchmark	Model (MB)	Size
googlenet [40]	6.89		inception [40]	24.36	
mobilenet [40]	3.63		resnet [40]	11.84	
shufflenet [40]	2.56				

TABLE V
A DESCRIPTION OF NEURAL NETWORK BENCHMARKS

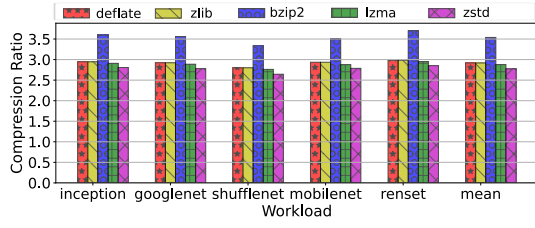


Fig. 3. Characterization of the compression algorithms (on the basis of the compression ratio)

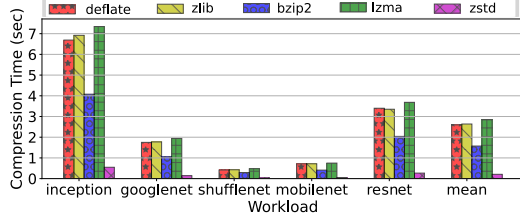


Fig. 4. Characterization of the compression algorithms (on the basis of the compression time)

B. Characterization of Chaotic Maps

The objective of this experiment is to determine and select the chaotic maps that have the lowest correlation coefficients and map generation times. The correlation coefficient (CC) measures the linear relationship between the two datasets. We compute the *Pearson's correlation coefficient* (CC) as $\frac{cov(X,Y)}{\sigma_X \times \sigma_Y}$. Here, $cov(X, Y)$ represents the covariance between the variables X and Y , while σ represents the standard deviation. A high correlation coefficient represents a strong relationship between the variables and vice-versa.

We selected the most popular chaotic maps for characterization as shown in Table VI. We performed experiments to estimate the constant values, which would result in chaotic behavior by estimating the Lyapunov Exponent (LE) as presented in Table VI.

Thereafter, we used the constants to generate the chaotic maps and performed a XOR operation between the maps and the weights. We present the results in Figures 5 and 6. We found that the *Chirikov* map is one of the slowest maps due to repeatedly computing the sine function.

Benchmark	Constants	LE
Henon [67] (2D)	$a=1.4; b=0.3$	0.61
Tent [16] (1D)	$\mu=1.98$	0.68
Logistic [50] (1D)	$\mu=3.98$	0.63
Lorenz [45] (3D)	$\sigma=10, \rho=28, \beta=-2.67$	0.92
Chirikov [13] (2D)	$k=10$	0.85

TABLE VI
CONTROL PARAMETERS OF CHAOTIC MAPS

We choose three maps based on the results: *Logistic*, *Lorenz*, and *Henon*. The *Logistic* and *Lorenz* maps have the fastest map generation times. The *Henon* map takes longer to generate but its correlation coefficient is the second lowest (after *Lorenz*). We did not choose *Chirikov* because of its slow generation



Fig. 5. Characterization of the chaotic maps (on the basis of the correlation coefficient)

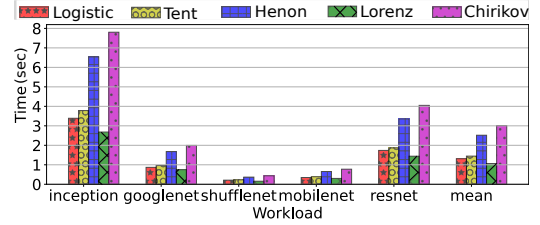


Fig. 6. Characterization of the chaotic maps (on the basis of the map generation time)

time and *Tent* because of its low performance and high correlation coefficient.

Conclusion: The most appropriate choices are the *Logistic*, *Lorenz*, and *Henon* maps. Among compression algorithms, *zstd* is the fastest with a good compression ratio.

V. DESIGN IMPLEMENTATION

A. Overview

The *SecOComp* hardware (SCE engine) consists of a permutation engine, a compression engine, a XOR-based substitution engine, and three compact hardware circuits that correspond to the chaotic map generators (see Figure 8).

We used the *zstd* compression engine from [11] and combined it with our proposed hardware, which simultaneously pre-computes chaotic maps while DRAM reads and compression engine operations are going on. Let us elaborate. Please keep referring to Figure 7 and 8.

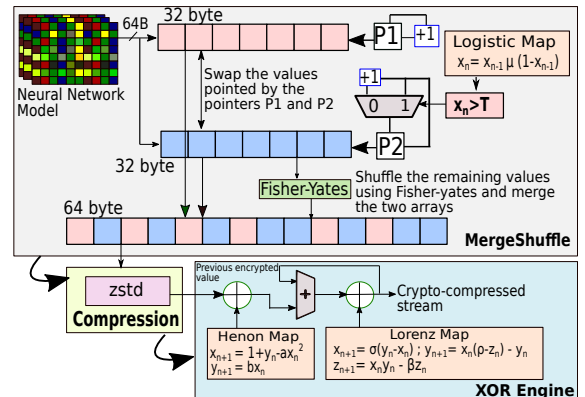


Fig. 7. Overall proposed scheme

Algorithm 1 Permutation using chaotic maps

Input: Intermediate data array $B = B_1, B_2, \dots, B_{64}$; secret Threshold T

Output: Permuted array B

```
Initialize  $K[0] = k_0$ ;  $srt = 1$ ;  $mid = 32$ ;  $end = 64$ 
\* Keep on iterating until one of the arrays is shuffled \*
while ( $srt \neq 32$  &  $mid \neq 64$ ) do
   $L1 = LogisticMap()$ 
  if  $L1 > T$  then
     $switch(B[srt], B[mid])$ 
    \* Switch the values stored in the locations pointed by
    the srt and mid \*
     $mid \leftarrow mid + 1$ 
  end if
   $srt \leftarrow srt + 1$ 
end while
\* Merge the remaining values in the undepleted array using
the Fisher-Yates algorithm \*
while  $mid \neq 64$  do
   $pos = LogisticMap() \% (mid, 64)$ 
   $switch(B[mid], B[pos])$ 
   $mid \leftarrow mid + 1$ 
end while
Return  $B$ 
```

B. Data Pre-processing and Quantization: Step (1)

① The service provider/owner of the model trains an NN model and quantizes its weights and biases. It sends the appropriately quantized values to the SCE engine for further compression and encryption. The quantization process is performed by the model owner before the data is written to memory. We assume that the hardware is aware of the data storage pattern of the NN model (standard assumption).

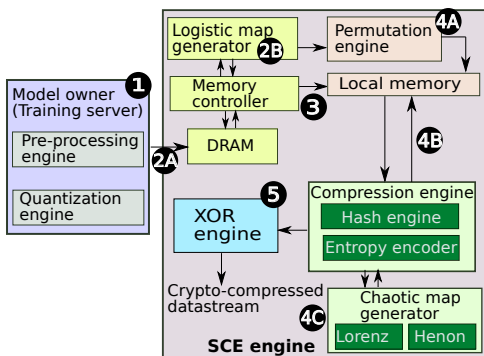


Fig. 8. A high-level design of the scheme

C. Data Read and Shuffling: Steps (2A), (2B), (3), and (4A)

②A The controller reads the weights from the DRAM and
②B simultaneously generates a *Logistic* map. The aim of doing this is to permute the values read from DRAM according to the values stored in the *Logistic* map. We achieve three

major benefits from this scheme: First, the map generation delay is subsumed in the shadow of DRAM reads. Second, permutation has little impact on the statistical features of data; this keeps the compression ratio intact. Third, due to the simultaneous map generation and DRAM reads, the micro-architectural signatures get distorted; this reduces side-channel leakage.

③ We store this data in a local memory for subsequent computations. Before the compression engine can compress this ‘ordered data’, it is shuffled (permuted). For permutation, we use the *MergeShuffle* [6] algorithm. The algorithm is shown in Algorithm 1. We divide a 64-byte block into two equal 32-byte chunks. We associate two pointers (starting at 0) with these two chunks. The *Logistic* map acts as a random number generator – the i^{th} Boolean random number is generated by comparing the i^{th} byte of the *Logistic* map with a secret threshold, T . If it is not equal, we swap the values indexed by the pointers and increment the pointers, otherwise we just increment one pointer without swapping. Ultimately, when one pointer reaches the end of a chunk, the remaining elements of the other chunk are permuted using the *Fisher-Yates* algorithm [6].

④A This procedure is repeated for all subsequent DRAM reads. The procedure of shuffling is straightforward and does not appear in the critical path of the system because it completely overlaps with the process of compression. Furthermore, the permutation engine operates at a higher frequency as compared to the compression engine, and while the compression of the current data bytes is taking place, the next chunk of data is fetched and permuted. Our tests show that this solution is necessary for creating a robust encryption algorithm and it also helps us maintain a good compression ratio.

D. Compression Engine: Step (4B)

④B The compression module reads the shuffled weight values from the local memory. The module comprises two main stages: a compression stage (performed using hash engines) and an entropy encoding stage. The readers can refer to [11] for a detailed architecture of the compression engine. In this work, we use a single compression unit. Our design can support many units as well.

E. Substitution Engine: Steps (4C) and (5)

We use a combination of two chaotic maps for substitution: the 2-D *Henon* map and the 3-D *Lorenz* map. Experiments demonstrated that a single map is insufficient to encrypt the weights, as the weights encrypted using a single map fail to provide sufficient encryption. This motivated us to use a combination of chaotic maps (similar to previous work [5]). We choose the *Logistic* map for permutation prior to compression because it is very fast and preserves important statistics about the data (given its high correlation coefficient). On the other hand, *Lorenz* and *Henon* are two strong maps with a low correlation coefficient; their combination allows us to create a strong substitution engine. We are free to use the strong maps

since the substitution is performed after the compression and the maps will have no impact on the compression ratio.

The encrypted initial values and the control parameters for the maps’ generation are read from the DRAM. The chaotic map generators will continue to generate the values until they receive an interrupt from the compression engine to either pause or finish the value generation process.

④C As soon as the compression begins, a *start* signal is transmitted to both the map generators – *Henon* and *Lorenz*. The **benefit** of this strategy is that the map generation process overlaps with the compression operation. A faster clock running at a 1 GHz frequency is used to generate the maps.

The maps generate 32-bit fixed-point values that are converted to 8-bit values as the weights are of size 1 byte (same as the previous work [5]). Thus, 8 LSB bits are extracted from the 32-bit values and are then used to encrypt the weights.

⑤ The encryption is performed using XOR gates and adders. The compressed information is XORed with the *Henon* map. Following this, the generated value is added to the previous crypto-compressed value, and the result is again XORed with the *Lorenz* map. This operation generates the next crypto-compressed value.

F. Simultaneous Decompression and Decryption Unit

The simultaneous decompression and decryption unit is simply a inverse of the SCE engine. We re-generate the same chaotic maps (*Lorenz* and *Henon*) using the same initial values and control parameters; these maps are XORed with the crypto-compressed datastream.

Then, decompression is performed to generate the de-compressed data. In the end, we re-generate the *Logistic* map using the same initial conditions and the control parameters in order to de-shuffle the de-compressed data. This procedure will produce the actual data. Given that we used fixed-point arithmetic, this process is deterministic and portable across ALU designs.

VI. EVALUATION

In this section, we perform a thorough performance evaluation of the proposed scheme and compare with a few recent proposals. We show all the evaluated configurations in Table VII. E1 is an ETC scheme with *zstd* and AES (Cipher-Block Chaining (CBC) mode). C1 is a CTE scheme that is the reverse of E1. C2 [65] uses a chaotic encryption-based CTE scheme and *zstd* for compression. S1 is the state-of-the-art in the SCE community proposed by Ahmad et al. [5]. *SecOComp* is our implementation, which has four specialized configurations of the form *Sec_XYZ*, where *XYZ* is the compression algorithm. Note that *zstd* is the default and is used with *SecOComp*.

A. Comparative Analysis (Software)

1) *A comparison with S1 and C2 (related work)*: We used the setup shown in Table IV. We observe a 70% improvement in the execution time and a $1.28\times$ better compression ratio using *SecOComp* as compared to S1 [5] (see Figures 9a and 9b). The main reasons behind the performance deterioration

in S1 are as follows ① In order to perform the permutation, they need to sequentially iterate through the entire dataset two times. This results in a significant performance overhead, particularly, if the dataset is large. However, in *SecOComp*, only one iteration is required to perform the permutation.

To improve the speed of Huffman coding, the authors in S1 use the *Chinese Remainder Theorem (CRT)* to transform adjacent data elements into a unique CRT solution. ② The authors pre-compute the unique solutions of the CRT for two 8-bit values and store the resultant 16-bit solution in a look-up table (LUT). The size of the LUT is estimated to be $2^8 \times 2^8 \times 16$ bits = 2^{20} bits = 128 kB, which is too large to fit in the caches, leading to a high number of cache misses.

It is essential to assess the effectiveness of integrating chaos-based encryption with a conventional compression technique for CTE configurations, we next compare with C2. We first perform the compression using *zstd* and then encrypt the data using the chaos-based scheme proposed by Wang et al. [65]. We observe that *SecOComp* results in nearly the same compression ratio as C2 [65]. However, *SecOComp* is $24\times$ faster than C2 [65]. The reasons for the poor performance of C2 [65] are as follows ① The algorithm is optimized for images (like most of the chaos-based encryption algorithms). In order to reduce the performance overheads, the complex computations (strong encryption) are performed on a specified region, which is identified by the *Region of Interest (ROI)*. For the non-ROI regions, a weaker encryption method is utilized. However, while working with NNs, we must assume that the ROI represents the entire model, as no information regarding the model can be leaked. This results in very high performance overheads. ② Due to the involvement of the *sine* function, the generation of the chaotic map takes a considerable amount of time. This map is used in the encryption of both ROI and non-ROI regions. ③ The third reason is that the encryption strategy is quite complex and requires a lot of sequential stages that are not hardware-friendly. As a result, the approach results in very poor performance when applied to NN model parameters.

Config.	Description
E1	An ETC scheme where <i>zstd</i> and AES-CBC is used
C1	A CTE scheme where <i>zstd</i> and AES-CBC is used
C2 [65]	A CTE scheme where the encryption scheme is proposed by Wang et al. [65]. For a fair analysis, We added <i>zstd</i> for compression
S1 [5]	The SCE scheme proposed by Ahmad et al. [5]
<i>SecOComp</i>	The proposed SCE implementation
<i>Sec_deflate</i>	<i>SecOComp</i> encryption + deflate compression
<i>Sec_gzip</i>	<i>SecOComp</i> encryption + <i>gzip</i> compression
<i>Sec_bzip</i>	<i>SecOComp</i> encryption + <i>bzip</i> compression
<i>Sec_lzma</i>	<i>SecOComp</i> encryption + <i>lzma</i> compression

TABLE VII

THE DIFFERENT DESIGN CONFIGURATIONS IMPLEMENTED IN THE PAPER

2) *A fair comparison between CTE, ETC and SecOComp Schemes*: We implemented our scheme *SecOComp* along with the baseline CTE (C1) and ETC (E1) schemes for performing a fair comparative analysis between the three schemes. We used Intel’s AVX (SIMD 256-bit [24]) instructions for further reducing the execution time. We selected the AES-CBC [18])

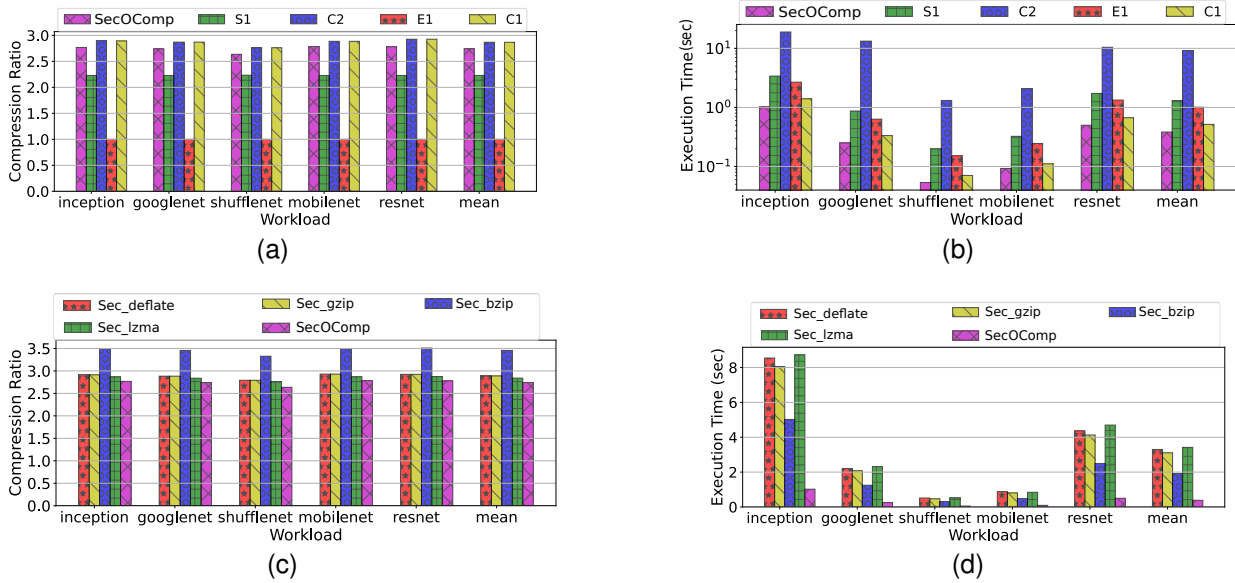


Fig. 9. A comparison (software-based) on the basis of the (a) compression ratio for various configurations. (b) execution time of various configurations (c) compression ratio for *SecOComp* configurations (d) execution time of *SecOComp* configurations

openssl implementation for the ETC and CTE implementations as it is the most popular and secure cipher according to the NIST standards, and we selected the *zstd* compression scheme for a fair analysis. We present the results in Figures 9a and 9b.

We observed that the ETC scheme results in a very poor compression ratio, while CTE results in a marginally increased compression ratio (+1.83%). Note that although we have utilized the same compression algorithm in both the *SecOComp* and CTE schemes, the weights in our scheme were permuted before compression. This leads to a 1.83% decrease in the compression ratio, which is minimal. Additionally, our scheme is 82% faster than ETC and 30.4% faster than CTE.

It is clear that ETC schemes are ineffective. As a result, we shifted our focus to different compression schemes using *SecOComp* (of the form *Sec_XYZ*).

3) *A comparison with other SecOComp configurations:* We study the impact of modifying the type of compression scheme on the compression ratio and the execution time of *SecOComp* (see Figures 9c and 9d). We observe that *SecOComp* is 8.62 \times , 8.11 \times , and 8.92 \times faster than *Sec_deflate*, *Sec_gzip*, and *_lzma*, respectively. *SecOComp* leads to only a 3.6% reduction in the compression ratio as compared to *Sec_lzma* with a 8.92 \times speedup. *Sec_bzip* leads to the best compression ratio but the scheme is 4.99 \times slower than *SecOComp*. The results can easily be correlated with our characterization results (see Section IV).

B. Hardware Implementations of *SecOComp* and CTE

We selected the two best schemes (*SecOComp* and C1) in terms of the execution time and the compression ratio, respectively, and implemented them in hardware. The code for *SecOComp* and CTE(C1) was written in VHDL 2008.

We synthesized, placed, and routed the designs using the Cadence Genus tool at the 28 nm ASIC technology node. The compression engine operates at a frequency of 300 MHz, while the permutation and substitution engines operate at 1 GHz. Table VIII presents the area and power results for each module. Figure 10 shows a comparison of the execution time in HW. We observe a 23.5% improvement in the execution time (for *SecOComp*), 19.8% area improvement as well as a 26.11% improvement in power consumption as compared to C1.

Module	Area($\mu\text{m}^2 \times 10^3$)	Power(mW)
<i>SecOComp</i>		
Permutation	0.89	0.06
Compression (zstd)	112.91	10.83
Substitution	2.26	0.17
Total	116.06	11.06
C1		
Compression (zstd)	112.91	10.83
AES-128	31.9	4.14
Total	144.81	14.97
Tool	Cadence RTL Compiler, 28 nm	

TABLE VIII
ASIC RESOURCE AND POWER UTILIZATION FOR VARIOUS COMPONENTS FOR *SecOComp* AND C1

VII. SECURITY ANALYSIS

The security of a system can be demonstrated using one of four basic approaches ① statistical testing (e.g. NIST tests), ② resistance to known attacks, ③ proof by reduction, and ④ disclosing the scheme to the public, and waiting for an adversary to mount an attack (if possible). A common approach for establishing the security of any algorithm is by proof by reduction. We rely on the fact that a standard problem *A* is extremely difficult to solve. We establish the fact that

Scheme	Key sensitivity ($\times 10^{-3}$)							
	CSI				Pearson Coefficient			
	SecOComp	S1 ($\times 10^3$)	C2	AES	SecOComp	S1 ($\times 10^3$)	C2	AES
Inception	0.256	0.076	0.579	0.074	0.260	0.076	0.124	0.028
Googlenet	0.033	0.072	0.213	0.317	0.041	0.072	0.171	0.274
Shufflenet	0.212	0.069	0.237	0.510	0.220	0.069	0.195	0.458
MobileNet	0.426	0.061	-0.102	-0.181	0.413	0.061	-0.140	-0.222
Squeezenet	0.027	0.078	-0.330	0.018	0.033	0.078	0.290	0.027
Average	0.198	0.067	0.291	0.220	0.193	0.071	0.184	0.201

Dataset	Plaintext sensitivity ($\times 10^{-3}$)							
	CSI				Pearson Coefficient			
	SecOComp	S1 ($\times 10^3$)	C2 ($\times 10^3$)	AES	SecOComp	S1 ($\times 10^3$)	C2 ($\times 10^3$)	AES
Inception	0.616	-0.065	0.124	0.171	0.614	-0.094	0.124	0.125
Googlenet	0.286	-0.384	0.043	0.413	0.285	-0.416	0.043	0.369
Shufflenet	0.609	-2.520	0.125	0.552	0.611	-2.528	0.125	0.615
MobileNet	0.289	1.420	0.043	-0.452	0.249	1.372	0.043	-0.895
Squeezenet	0.443	-2.901	0.125	0.287	0.441	-2.904	0.124	0.333
Average	0.442	1.456	0.092	0.390	0.438	1.458	0.091	0.479

TABLE IX

KEY AND PLAINTEXT SENSITIVITY ANALYSIS

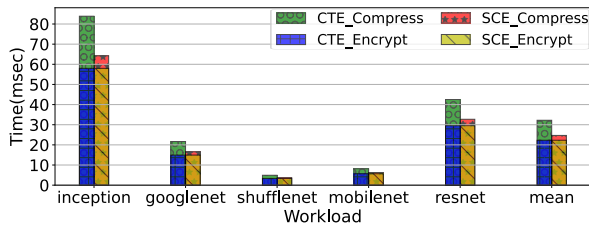


Fig. 10. A comparison (HW implementation) of the execution time for SecOComp and C1

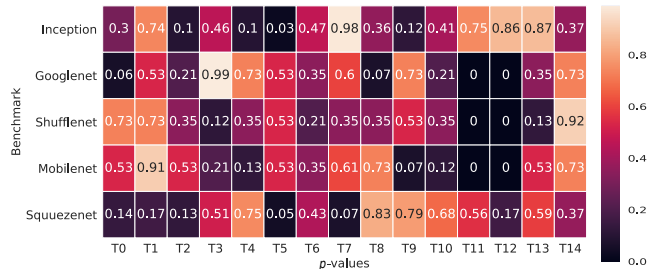
the problem A is reducible to B . If solving A is difficult, then solving B must be equally or more difficult as well. Sadly, there is no known standard solution in this domain for chaos-based encryption. This makes it hard for us to apply proof by reduction. The remaining strategies are discussed in detail in the next subsections. Our analysis subsumes analyses performed in prior work, especially recent work done on chaos-based encryption in the HW community [55], [64], [41], [34], [47], [65], [66], [51], [14], [17], [56], [21], [5].

A. NIST Tests

We performed all the tests specified in the NIST suite as shown in Table III. A test is successful if the p -value is greater than a threshold α (set to 0.01 on the lines of prior work [59]). We used 100 chunks of data (samples) of a length of 1 million each (for *inception* and *squeezenet*). However, because the model sizes of the other benchmarks is small, we used only 10 samples with a length of 1 million [59]. We were unable to achieve the p -value for the *random excursions* and *random excursions variant* tests (shown as 0 in the heatmap) as these tests are not applicable because they require a minimum sample length of 1 million and to get a valid p -value, we require at least 55 samples [59]. Figure 11 shows the heatmap of p -values of all the tests computed using the NIST test suite. The pass rate (# samples passing the test/total # of samples)

of all the tests varies between 0.98 – 1.0, which indicates that SecOComp passes all the 15 NIST tests. This is as per the documentation provided along with the test suite.

We also performed all the NIST tests on the ciphertexts generated by the schemes E1, C1, C2 and S1. We observed that the S1 scheme successfully passed 11/15 NIST tests. On the contrary, C2 failed several NIST tests. We also need to note that E1 and C1 passed all the NIST tests as they simply encapsulate AES-CBC.

Fig. 11. NIST Tests for SecOComp- A heatmap depicting the p -values for various benchmarks. A p -value $> \alpha$ signifies that the scheme passed the test.

B. Correlation Coefficient (CC) Analysis

The CC allows us to assess the degree of similarity between the plaintext and the ciphertext. The degree of similarity increases as the correlation value increases. In order to perform a correlation analysis, we calculate the *Pearson correlation coefficients* (using Equation 2) between the plaintexts and the ciphertexts generated using AES-CBC (covers C1 and E1), S1, C2 and SecOComp. We show the results in Table X. An efficient encryption technique will result in a correlation coefficient with a very low absolute value. We observe that SecOComp can provide similar levels of encryption as the AES-CBC cipher.

Scheme	Correlation Coeff. ($\times 10^{-3}$)			
	AES-CBC	S1	C2	SecOComp
Inception	0.017	0.144	0.199	0.151
Googlenet	0.161	0.554	-0.140	0.039
Shufflenet	0.191	-0.317	0.777	0.025
MobileNet	0.215	-0.607	0.759	0.285
SqueezeNet	0.161	0.380	-0.188	0.269
Average	0.151	0.400	0.425	0.153

TABLE X
CORRELATION BETWEEN THE PLAINTEXT AND CIPHERTEXT IN
AES-CBC, S1, C2 AND *SecOComp*

C. Key Space Analysis

The Kerckhoff’s principle states that the security of an algorithm should be dependent only on the secret key. An efficient encryption algorithm should have a large keyspace that is resistant to brute-force attacks [5], [65], [58]. In general, the keyspace is the product of the number of possible subkeys used in each phase of the algorithm. $K_S = \prod K_i$, where K_S is the keyspace and K_i is the number of subkeys in each phase of the algorithm. Our proposed technique is based on a permutation-and-substitution procedure involving three chaotic maps. Thus, our key consists of three components: the permutation key K_p and the XOR engine keys K_{s1} and K_{s2} . K_p is composed of one initial condition (corresponding to the *Logistic* map), one secret parameter (μ) and a secret threshold value. Key K_{s1} consists of two initial conditions (corresponding to the *Henon* map) and two secret parameters (a , b), whereas key K_{s2} consists of three initial conditions (corresponding to the *Lorenz* map) and three secret parameters (σ , ρ , β). The computational precision of 32-bit fixed point number is approximately 10^8 .

The total keyspace of the proposed scheme can be written as (approximately): $K_S = K_{s1} \times K_p \times K_{s2} = 10^{8 \times 7 + 6 \times 8} = 10^{104}$.

D. Sensitivity Analysis

We perform a sensitivity analysis to examine the impact of a little modification in the plaintext or the secret key on the entire ciphertext (referred to as *diffusion* and *confusion*, respectively). In line with the prior work, we use the *Pearson’s correlation coefficient (CC)* and the *Cosine Similarity Index (CSI)*. CSI is a metric that is used to measure the similarity between two vectors. It is computed as $\frac{X \cdot Y}{|X| \times |Y|}$. The value of CSI lies between -1 and 1. The lower the magnitude of the value, the lower the correlation between the two datasets. We use the in-built function from the *sklearn 0.24.1* library [3] to compute the CSI.

1) *Key Sensitivity Analysis* : The key sensitivity analysis determines the effect of a 1-bit change in the key on the ciphertext. We use the CSI and CC to compare the similarity of ciphertexts generated by changing a single bit of the key as shown in Table IX. We compare the results with the most recent SCE implementation S1, C2 and AES-CBC (covers C1 and E1). We observe that our values are nearly the same as the AES-CBC.

2) *Plaintext Sensitivity (Avalanche Effect) Analysis* : Similar to the key sensitivity analysis, plaintext sensitivity indicates the effect of a single-bit change in the plaintext on the ciphertext. An encryption method must produce fully distinct ciphertexts from a group of plaintexts containing small changes. We examine the similarity between the ciphertexts generated by altering a single bit of the plaintext using the CSI and CC as shown in Table IX. We observe similar results as the earlier experiment.

E. Classical Attacks

There are some well-known classical attacks in the crypt-analysis literature, such as the ❶ *Known Plaintext Attack* where an attacker *knows* plaintexts and the corresponding ciphertexts. ❷ *Chosen Plaintext Attack* where an attacker can select a plaintext to pass through the encryption algorithm and obtain its corresponding ciphertext. ❸ *Chosen Ciphertext Attack* where an attacker can choose a ciphertext to pass through the decryption algorithm and obtain its corresponding plaintext. ❹ *Only Ciphertext Attack* where an attacker has an access to ciphertexts.

It has been theoretically proven that out of these attacks, the chosen plaintext attack is the most powerful [58]. Consequently, if a cryptosystem can withstand this attack, it can withstand other types of attacks as well. Several authors [58], [65], [23], [70] mention that if an algorithm has strong confusion and diffusion properties, they can withstand such attacks. The preceding section already demonstrated that *SecOComp* has significant confusion and diffusion.

F. Crypt-analysis of *SecOComp*

Chen et al. [12] propose a theoretical crypt-analysis framework for chaos-based encryption systems. This is the most recent and comprehensive work in this domain. The authors perform cryptanalysis on the algorithms, which satisfy the following property and outline methods to break them: $C_1 \oplus C_2 = Perm_K(P_1 \oplus P_2)$, where $C_i = Perm_K(P_i) \oplus K_1$. (C_1, C_2) and (P_1, P_2) are a pair of ciphertexts and the corresponding plaintexts, respectively. \oplus denotes a XOR operation, K_1 represents the secret key and $Perm_K$ denotes a permutation operation dependent on the secret key K . Fortunately, *SecOComp* does not satisfy the above-mentioned property because the ciphertext is a complex function of the compressed permuted data and the secret key. This statement of ours has been theoretically and experimentally validated.

G. Additional Results

We examine the efficiency and security of our scheme when applied to different types of datasets utilizing the identical system configuration described in Table IV.

1) *Datasets Description*: We demonstrate the effectiveness and security of our technique for various images. We investigated five standard images from the USC-SIPI Image Database[61]: *baboon*, *jelly*, *peppers*, *tank*, and *woman*. We also take into account other datasets, which are obtained from the official Kaggle website. The details of the datasets are

present in Table XI. Both the USC-SIPI Image dataset and the Kaggle dataset have received considerable attention from the scientific community and have been extensively used [49], [20], [60].

Dataset Description	Category	Size	Notation
Covid cases and deaths worldwide [26]	Healthcare	8 kB	D1
Top 1000 movies by IMDB rating [27]	User study	53 kB	D2
CO ₂ emission by country [31]	Weather	117 kB	D3
Data of 1000+ Amazon product's rating and reviews [30]	User study	2 MB	D4
3000 conversations dataset for chatbots [25]	Phone	69 kB	D5
Medical cost personnel datasets - Insurance forecast by using linear regression [28]	User study	16 kB	D6
Numerically generated ECG signal [29]	Healthcare	1 MB	D7

TABLE XI
DESCRIPTION OF THE DATASETS

2) *Performance and Security Analysis*: Figures 12 and 13 present the execution time and compression ratio for all the selected images. Figures 14 and 15 demonstrate the execution time and compression ratio for other datasets. We observe that *SecOComp* is able to provide an optimal ratio between the execution time and the compression ratio. We performed an extensive security analysis and we present the results in Tables XIII and XII. We also conducted NIST tests to evaluate the algorithm's security. We see that *SecOComp* passed all necessary NIST tests and can give adequate security guarantees.

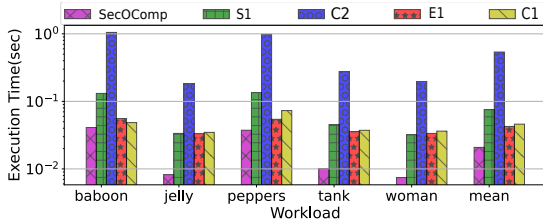


Fig. 12. A comparison of the execution time for different images

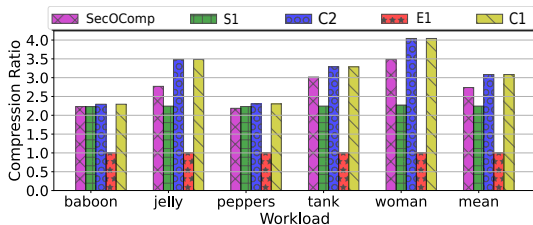


Fig. 13. A comparison of the compression ratio for different images

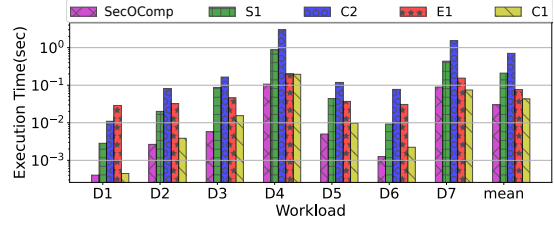


Fig. 14. A comparison of the execution time for different datasets

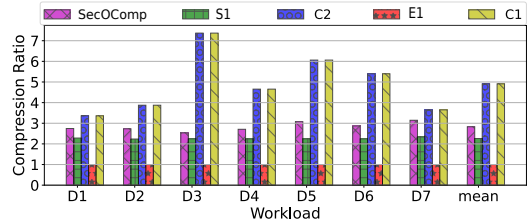


Fig. 15. A comparison of the compression ratio for different datasets

VIII. RELATED WORK

SCE schemes have been proposed in the context of images. Wang et al. [63] propose to simultaneously compress and encrypt an image by dividing the image channels (R, G, B) into blocks and perform compression sensing using chaotic maps. The image is further diffused using chaotic maps. Abaturab et al. [4] propose to simultaneously compress and encrypt images on similar lines. Four images are decomposed into four sub-bands by using wavelet transforms. They fuse the resulting sub-bands to make a single fused image, which is split into R, G, and B channels, which are subsequently compressed and encrypted. Ahmad et al. [5] propose using two chaotic maps and the Huffman coding system to simultaneously compress and encrypt the data. First, they propose a chaotic map to permute the data. Then, the adjacent values of the permuted data are represented as a unique solution of the CRT. These values are sent to the Huffman compressor for performing the compression operation. Finally, a *Logistic* map is used to perform a XOR operation. We showed that such algorithms have issues with performance and security.

Some other works [65], [5] rely on identifying a region of interest (ROI) containing the majority of the information content. Wang et al. [65] proposed separating the image into ROI and non-ROI regions, which would then be encrypted using different chaos-based encryption techniques. They use compute-intensive algorithms for the ROI-based region, which lead to a significant performance overhead. The non-ROI region was encrypted using a simpler scheme. This reduced the overall performance overhead. Sadly, the issue with NN models is that the entire model contains a great deal of intellectual property, which should be secured and thus the entire model is in the ROI. Hence, this approach is unsuitable for NN data.

Due to the large size of NNs, we require not only an efficient compression and encryption engine but also several architectural optimizations to speed up the entire process in hardware.

Dataset	Key sensitivity ($\times 10^{-2}$)							
	CSI				Pearson Coefficient			
	SecOComp	S1	C2	AES	SecOComp	S1	C2	AES
D1	-0.1010	0.5844	0.0393	0.7483	-0.1037	0.5805	0.0349	-0.0683
D2	0.0135	2.0347	0.5224	0.7477	-4.9005	2.0405	0.5243	-1.2372
D3	-0.0416	7.6540	0.0771	0.7484	-0.0411	7.6487	0.0705	-0.0381
D4	0.0212	6.4575	0.1252	0.7491	0.0172	6.4553	0.1222	0.1986
D5	0.0692	1.1027	-0.0305	0.7485	0.0662	1.0100	-0.0351	0.0663
D6	-0.2282	1.0739	-0.1131	0.7489	-0.2351	1.0735	-0.1152	-0.0202
D7	0.1219	9.5453	-1.2454	0.7489	0.1189	9.5470	-1.2559	0.1035
Images								
baboon	0.1884	8.2555	-0.0634	0.7481	0.1831	8.2542	-0.0693	-0.1135
jelly	0.1149	6.3944	0.0672	0.7479	0.1081	6.3907	0.0635	-0.0318
peppers	0.1096	6.4588	-0.0526	0.7485	0.1049	6.4563	-0.0584	-0.0523
tank	0.2192	6.5114	0.2410	0.7484	0.2134	6.5075	0.2356	-0.0569
woman	0.2126	0.3014	0.0984	0.7486	0.2114	0.2948	0.0937	0.0491
Plaintext sensitivity								
Dataset	CSI				Pearson Coefficient			
	SecOComp	S1	C2	AES	SecOComp	S1	C2	AES
D1	0.8385	-0.0515	0.0436	0.7486	0.8385	-0.0515	0.0436	0.0003
D2	0.0063	-0.0151	0.0460	0.7521	0.0061	-0.0151	0.0460	0.0019
D3	-0.0074	-0.0553	0.0432	0.7479	-0.0074	-0.0553	0.0432	-0.0009
D4	0.0039	-0.0520	0.0429	0.7485	0.0039	-0.0521	0.0429	0.0001
D5	0.0002	0.0774	0.1235	0.7485	0.0002	0.0774	0.1235	0.0002
D6	0.0014	-0.0095	0.1204	0.7491	0.0014	-0.0095	0.1203	0.0015
D7	-0.0089	-0.0223	0.0457	0.7503	-0.0091	-0.0223	0.0456	0.0002
Images								
baboon	0.0024	-0.0501	0.0433	0.7489	0.0024	-0.0501	0.0433	0.0016
jelly	-0.1538	-0.0233	0.1188	0.7469	-0.1539	-0.0233	0.1188	-0.0013
peppers	0.1254	-0.0208	0.0999	0.7487	0.1253	-0.0208	0.098	0.0011
tank	0.2912	-0.0217	0.0433	0.7484	0.2912	-0.0218	0.0433	-0.0011
woman	0.1029	-0.0039	0.1190	0.7473	0.1029	-0.0040	0.1189	-0.0032

TABLE XII
KEY AND PLAINTEXT SENSITIVITY ANALYSIS FOR DIFFERENT DATASETS

Dataset	Correlation Coeff. ($\times 10^{-2}$)			
	AES-CBC	S1	C2	SecOComp
D1	-0.396	3.141	-1.351	-0.248
D2	0.398	0.377	-0.129	0.092
D3	-0.017	0.970	0.137	0.219
D4	-0.020	0.226	0.070	-0.325
D5	-0.068	0.262	0.156	0.011
D6	0.128	-0.618	0.198	-0.097
D7	-0.188	-0.618	0.091	-0.021
Images				
baboon	0.106	3.394	-0.085	-0.868
jelly	-0.085	7.007	-0.125	1.878
peppers	0.006	-3.916	0.248	-0.177
tank	0.186	1.847	0.018	-1.135
woman	0.162	-0.959	-0.030	3.457

TABLE XIII
CORRELATION BETWEEN THE PLAINTEXT AND CIPHERTEXT IN AES-CBC, S1, C2 AND SecOComp

To the best of our knowledge, there is no SCE solution for NN data and there is no work in hardware optimizations to implement the same. Retrofitting SCE solutions proposed for images or intelligently combining different compression and encryption methods did not lead to an effective SCE scheme, hence, a bespoke solution *SecOComp* was proposed.

IX. CONCLUSION

In this study, we propose *SecOComp*, an SCE algorithm that is able to successfully [18] compress and encrypt any type of data. We relied on chaos-based encryption techniques because

a combination of different chaotic maps to create encryption algorithms has rejuvenated the area of chaotic cryptography, allowing us to easily realize a high level of security. We went a step further by combining chaotic cryptography with a compression technique. Performing some portion of encryption in the shadow of DRAM reads and compression operations allowed us to speed up the entire process and achieve not only good performance and security but also a decent compression ratio. We also evaluated state-of-the-art SCE solutions and showed that they are unsuitable for not only NN data but also for other miscellaneous data, and our bespoke solution *SecOComp* is secure, robust, and fast.

REFERENCES

- [1] "175 zettabytes by 2025," <https://www.forbes.com/sites/tomcoughlin/2018/11/27/175-zettabytes-by-2025/?sh=4904167c5459>, accessed: 2023-03-30.
- [2] "The data explosion and hidden data storage costs in the cloud – could object storage be the answer?" <https://www.lightedge.com/blog/the-data-explosion-and-hidden-data-storage-costs-in-the-cloud-could-object-storage-be-the-answer/>, accessed: 2023-03-30.
- [3] "Scikit-learn." [Online]. Available: <https://pypi.org/project/scikit-learn/>
- [4] M. R. Abuturab and A. Alfalou, "Multiple color image fusion, compression, and encryption using compressive sensing, chaotic-biometric keys, and optical fractional fourier transform," *Optics & Laser Technology*, 2022.
- [5] I. Ahmad and S. Shin, "A novel hybrid image encryption-compression scheme by combining chaos theory and number theory," *Signal Processing: Image Communication*, 2021.
- [6] A. Bacher *et al.*, "Mergeshuffle: a very fast, parallel random permutation algorithm," *arXiv:1508.03167*, 2015.

- [7] G. Balan, S. Arumugam, S. Muthusamy, H. Panchal, H. Kotb, M. Bajaj, S. S. Ghoneim *et al.*, "An improved deep learning-based technique for driver detection and driver assistance in electric vehicles with better performance," *International Transactions on Electrical Energy Systems*, vol. 2022, 2022.
- [8] S. Bharadwaj, "Using convolutional neural networks to detect compression algorithms," *arXiv preprint arXiv:2111.09034*, 2021.
- [9] O. Billet, H. Gilbert, and C. Ech-Chatbi, "Cryptanalysis of a white box aes implementation," in *International workshop on selected areas in cryptography*. Springer, 2004, pp. 227–240.
- [10] J. Bonneau, "Robust final-round cache-trace attacks against aes," *Cryptology ePrint Archive*, 2006.
- [11] J. Chen *et al.*, "Fpga acceleration of zstd compression algorithm," in *IPDPSW*. IEEE, 2021.
- [12] J. Chen, L. Chen, and Y. Zhou, "Cryptanalysis of image ciphers with permutation-substitution network and chaos," *IEEE Transactions on Circuits and Systems for Video Technology*, vol. 31, no. 6, pp. 2494–2508, 2020.
- [13] B. Chirikov and D. Shepelyansky, "Chirikov standard map," *Scholarpedia*, 2008.
- [14] K. Cho and T. Miyano, "Chaotic cryptography using augmented lorenz equations aided by quantum key distribution," *IEEE Transactions on Circuits and Systems I: Regular Papers*, vol. 62, no. 2, pp. 478–487, 2014.
- [15] Y. Collet. (2021) Zstd github repository from facebook. [Online]. Available: <https://github.com/facebook/zstd>
- [16] M. CRAMPIN and B. Heal, "On the chaotic behaviour of the tent map," *Teaching Mathematics and its Applications: An International Journal of the IMA*, 1994.
- [17] J. Cui, Y. Wang, J. Zhang, Y. Xu, and H. Zhong, "Full session key agreement scheme based on chaotic map in vehicular ad hoc networks," *IEEE Transactions on Vehicular Technology*, vol. 69, no. 8, pp. 8914–8924, 2020.
- [18] J. Daemen and V. Rijmen, "Reijndael: The advanced encryption standard." *Dr. Dobbs's Journal: S/W Tools for the Professional Programmer*, 2001.
- [19] P. Deutsch, "Deflate compressed data format specification version 1.3," Tech. Rep., 1996.
- [20] D. Herbadji, A. Belmeguenai, N. Derouiche, and H. Liu, "Colour image encryption scheme based on enhanced quadratic chaotic map," *IET Image Processing*, vol. 14, no. 1, pp. 40–52, 2020.
- [21] Z. Hua, Y. Zhang, H. Bao, H. Huang, and Y. Zhou, "n-dimensional polynomial chaotic system with applications," *IEEE Transactions on Circuits and Systems I: Regular Papers*, vol. 69, no. 2, pp. 784–797, 2021.
- [22] J. Huang, C.-X. Wang, L. Bai, J. Sun, Y. Yang, J. Li, O. Tirkkonen, and M.-T. Zhou, "A big data enabled channel model for 5g wireless communication systems," *IEEE Transactions on Big Data*, vol. 6, no. 2, pp. 211–222, 2018.
- [23] K. Jain, A. Aji, and P. Krishnan, "Medical image encryption scheme using multiple chaotic maps," *Pattern Recognition Letters*, vol. 152, pp. 356–364, 2021.
- [24] H. Jeong *et al.*, "Performance of sse and avx instruction sets," *arXiv:1211.0820*, 2012.
- [25] Kaggle. 3k conversations dataset for chatbot. [Online]. Available: <https://www.kaggle.com/datasets/kreeshrajani/3k-conversations-dataset-for-chatbot>
- [26] Kaggle. Covid cases and deaths. [Online]. Available: <https://www.kaggle.com/datasets/themrityunjaypathak/covid-cases-and-deaths-worldwide>
- [27] Kaggle. Imdb movies dataset. [Online]. Available: <https://www.kaggle.com/datasets/rajucg/imdb-top-250-movies-dataset>
- [28] Kaggle. Medical cost personal datasets. [Online]. Available: <https://www.kaggle.com/datasets/mirichoi0218/insurance>
- [29] Kaggle. Numerically generated ecg signal. [Online]. Available: <https://www.kaggle.com/datasets/ahmadsaeed1007/ecg-signal>
- [30] Kaggle. (2021) amazon product's ratings and reviews. [Online]. Available: <https://www.kaggle.com/datasets/karkavelrajaj/amazon-sales-dataset>
- [31] Kaggle. (2021) Co2-emissions-by-country. [Online]. Available: <https://www.kaggle.com/datasets/ulrikthygepedersen/co2-emissions-by-country>
- [32] H. G. Kim, H.-T. Lim, and Y. M. Ro, "Deep virtual reality image quality assessment with human perception guider for omnidirectional image," *IEEE Transactions on Circuits and Systems for Video Technology*, vol. 30, no. 4, pp. 917–928, 2019.
- [33] P. Kumar, R. Kumar, G. Srivastava, G. P. Gupta, R. Tripathi, T. R. Gadekallu, and N. N. Xiong, "Ppsf: A privacy-preserving and secure framework using blockchain-based machine-learning for iot-driven smart cities," *IEEE Transactions on Network Science and Engineering*, vol. 8, no. 3, pp. 2326–2341, 2021.
- [34] R. Lan, J. He, S. Wang, Y. Liu, and X. Luo, "A parameter-selection-based chaotic system," *IEEE Transactions on Circuits and Systems II: Express Briefs*, vol. 66, no. 3, pp. 492–496, 2018.
- [35] E. J. Leavline and D. Singh, "Hardware implementation of lzma data compression algorithm," *International Journal of Applied Information Systems (IIAIS)*, vol. 5, no. 4, pp. 51–56, 2013.
- [36] C. Li, Y. Liu, L. Y. Zhang, and M. Z. Chen, "Breaking a chaotic image encryption algorithm based on modulo addition and xor operation," *International Journal of Bifurcation and Chaos*, vol. 23, no. 04, p. 1350075, 2013.
- [37] C. Li, T. Xie, Q. Liu, and G. Cheng, "Cryptanalyzing image encryption using chaotic logistic map," *Nonlinear Dynamics*, vol. 78, pp. 1545–1551, 2014.
- [38] C. Li, L. Y. Zhang, R. Ou, K.-W. Wong, and S. Shu, "Breaking a novel colour image encryption algorithm based on chaos," *Nonlinear dynamics*, vol. 70, pp. 2383–2388, 2012.
- [39] Y. Li, L. Ma, Z. Zhong, F. Liu, M. A. Chapman, D. Cao, and J. Li, "Deep learning for lidar point clouds in autonomous driving: A review," *IEEE Transactions on Neural Networks and Learning Systems*, vol. 32, no. 8, pp. 3412–3432, 2020.
- [40] Z. Li *et al.*, "A survey of convolutional neural networks: analysis, applications, and prospects," *IEEE trans. on neural netw learn syst*, 2021.
- [41] N. Lin, X. Chen, H. Lu, and X. Li, "Chaotic weights: A novel approach to protect intellectual property of deep neural networks," *IEEE Transactions on Computer-Aided Design of Integrated Circuits and Systems*, vol. 40, no. 7, pp. 1327–1339, 2020.
- [42] Y. Ma, C. Li, and B. Ou, "Cryptanalysis of an image block encryption algorithm based on chaotic maps," *Journal of Information Security and Applications*, vol. 54, p. 102566, 2020.
- [43] K. Marton and A. Suci, "On the interpretation of results from the nist statistical test suite," *Science and Technology*, 2015.
- [44] M. McComb, R. Bies, and M. Ramanathan, "Machine learning in pharmacometrics: Opportunities and challenges," *British Journal of Clinical Pharmacology*, vol. 88, no. 4, pp. 1482–1499, 2022.
- [45] L. Merah *et al.*, "Design and fpga implementation of lorenz chaotic system for information security issues," *Applied Mathematical Sci.*, 2013.
- [46] N. Munir *et al.*, "Cryptanalysis of internet of health things encryption scheme based on chaotic maps," *IEEE Access*, 2021.
- [47] A. Nourian and M. Maheswaran, "Towards privacy enhanced limited image processing in the clouds," in *Proceedings of the 9th Middleware Doctoral Symposium of the 13th ACM/IFIP/USENIX International Middleware Conference*, 2012, pp. 1–6.
- [48] OpenAI, "Chatgpt," 2022. [Online]. Available: <https://openai.com/blog/chatgpt/>
- [49] H. Pouransari and S. Ghili, "Deep learning for sentiment analysis of movie reviews," *CS224N Proj*, pp. 1–8, 2014.
- [50] S. Rabinovich *et al.*, "logistic map": an analytical solution," *Physica A: Statistical Mechanics and its Applications*, 1995.
- [51] M. U. Rehman, A. Shafique, Y. Y. Ghadi, W. Boulila, S. U. Jan, T. R. Gadekallu, M. Driss, and J. Ahmad, "A novel chaos-based privacy-preserving deep learning model for cancer diagnosis," *IEEE Transactions on Network Science and Engineering*, vol. 9, no. 6, pp. 4322–4337, 2022.
- [52] N. Shrivastava and S. R. Sarangi, "Towards an optimal countermeasure for cache side-channel attacks," *IEEE Embedded Systems Letters*, 2022.
- [53] N. Shrivastava and S. R. Sarangi, "Securator: A fast and secure neural processing unit," in *29th International Symposium on High-Performance Computer Architecture (HPCA)*. IEEE, 2023.
- [54] J. Soto and J. Soto, *Randomness testing of the advanced encryption standard candidate algorithms*. US Dept. of Commerce, Tech. Administration, National Institute of ..., 1999.
- [55] J. Srinivas, A. K. Das, M. Wazid, and N. Kumar, "Anonymus lightweight chaotic map-based authenticated key agreement protocol for industrial internet of things," *IEEE Transactions on Dependable and Secure Computing*, vol. 17, no. 6, pp. 1133–1146, 2018.

- [56] J. Srinivas, A. K. Das, M. Wazid, and N. Kumar, "Anonymous lightweight chaotic map-based authenticated key agreement protocol for industrial internet of things," *IEEE Transactions on Dependable and Secure Computing*, vol. 17, no. 6, pp. 1133–1146, 2018.
- [57] Z. B. Tariq, N. Arshad, and M. Nabeel, "Enhanced lzma and bzip2 for improved energy data compression," in *2015 International Conference on Smart Cities and Green ICT Systems (SMARTGREENS)*. IEEE, 2015, pp. 1–8.
- [58] N. Tsafack, S. Sankar, B. Abd-El-Atty, J. Kengne, K. Jithin, A. Belazi, I. Mehmood, A. K. Bashir, O.-Y. Song, and A. A. Abd El-Latif, "A new chaotic map with dynamic analysis and encryption application in internet of health things," *IEEE Access*, vol. 8, pp. 137 731–137 744, 2020.
- [59] K. H. Tsoi *et al.*, "High performance physical random number generator," *IET computers & digital techniques*, 2007.
- [60] I. Ullah, U. Hayat, and M. D. Bustamante, "Image encryption using elliptic curves and rossby/drift wave triads," *Entropy*, vol. 22, no. 4, p. 454, 2020.
- [61] USC. The usc-sipi image database. [Online]. Available: <https://sipi.usc.edu/database/database.php?volume=misc>
- [62] H. Wang, D. Xiao, X. Chen, and H. Huang, "Cryptanalysis and enhancements of image encryption using combination of the 1d chaotic map," *Signal processing*, vol. 144, pp. 444–452, 2018.
- [63] K. Wang *et al.*, "Double color images compression–encryption via compressive sensing," 2021.
- [64] W. Wang, Z. Han, M. Alazab, T. R. Gadekallu, X. Zhou, and C. Su, "Ultra super fast authentication protocol for electric vehicle charging using extended chaotic maps," *IEEE Transactions on Industry Applications*, vol. 58, no. 5, pp. 5616–5623, 2022.
- [65] X. Wang and P. Liu, "A new full chaos coupled mapping lattice and its application in privacy image encryption," *IEEE Transactions on Circuits and Systems I: Regular Papers*, vol. 69, no. 3, pp. 1291–1301, 2021.
- [66] Y. Wang, Z. Liu, L. Y. Zhang, F. Pareschi, G. Setti, and G. Chen, "From chaos to pseudorandomness: A case study on the 2-d coupled map lattice," *IEEE Transactions on Cybernetics*, 2021.
- [67] H. Wen, "A review of the hénon map and its physical interpretations," *School of Physics Georgia Institute of Technology, Atlanta, GA*, 2014.
- [68] E. Y. Xie, C. Li, S. Yu, and J. Lü, "On the cryptanalysis of fridrich's chaotic image encryption scheme," *Signal processing*, vol. 132, pp. 150–154, 2017.
- [69] L. Zhang, "Hénon map chaotic system analysis and vhdl-based fixed-point fpga implementation for brain stimulation," in *CCECE*, 2017.
- [70] M. Zhang, X.-J. Tong, J. Liu, Z. Wang, J. Liu, B. Liu, and J. Ma, "Image compression and encryption scheme based on compressive sensing and fourier transform," *IEEE Access*, vol. 8, pp. 40 838–40 849, 2020.